Four-Terminal Pair Digital Sampling Impedance Bridge up to 1 MHz

Stanislav Mašláň, Martin Šíra, Tereza Skalická, and Tobias Bergsten

***Abstract*— This paper describes a new four-terminal pair (4TP) digital sampling impedance bridge designed for the frequency range up to 1 MHz and small impedances, such as shunts. The bridge is capable of comparing impedance standards of arbitrary ratios in a full complex plane from approximately 100 kΩ down to 50 mΩ, limited by the maximum achievable current 3 A. To keep low uncertainties, a new multiplexer was designed and a very simple and fully automated linearity correction method based on the pair of calculable resistors was developed and validated. This paper describes the design and details of the bridge topology, basic uncertainty budget, and first results of the validation. The expanded uncertainty of impedance module is about 50 µΩ/Ω at 1 MHz for impedance ratios up to 1:16 and voltage drops above 10 mV and the expanded uncertainty of a phase angle was about 360 µrad/MHz. Expanded uncertainty for frequency 100 kHz about 10 µΩ/Ω was reached. Typical expanded uncertainty for low-impedance ratios below 1:1.1 is only 35 µΩ/Ω. Set of measurement of impedance standards of known values and a small international comparison of ac–dc and phase angle errors of current shunts were carried out to validate the bridge capabilities in a wide range of impedances. The validation measurements showed the deviations of the bridge are below 35 µΩ/Ω and below 350 µrad at 1 MHz.**

***Index Terms*— Bridge circuits, impedance measurement, phase comparators, sampling methods, shunts (electrical).**

I. Introduction

ELECTRICAL impedance metrology plays a significant role in the characterization of components of various measurement systems. Example of such field is power and power quality metrology where it is being used to calibrate current shunts in terms of ac resistance and phase angle errors. Numerous calibration methods were presented at the lower frequency band up to few tens of kilohertz. However, recent customer demands extended to frequencies over 100 kHz. Furthermore, customers recently require calibration of general impedance standards in a frequency range up to at least 1 MHz with improved uncertainty.

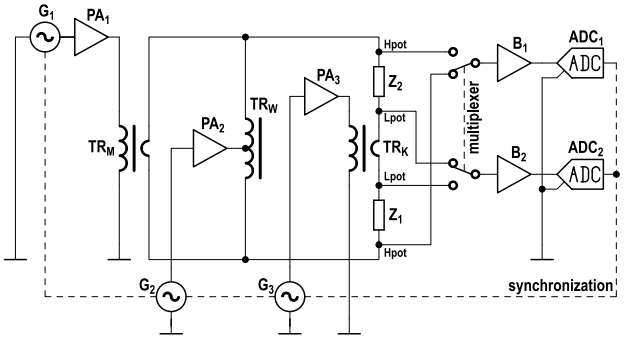

Fig. 1. Principal circuit diagram of the digital sampling impedance bridge.

First, major group of bridges capable to partially cover the demand is coaxial bridges of classic design with inductive voltage dividers (IVDs). Several bridges of this type capable of operation at or above 1 MHz were presented in past decades, such as [1] and [2]. However, these are not suitable for frequent customer calibrations as they require time-consuming manual balancing. A digitally assisted modification of such designs was presented in [3]. Although these bridges still offer the best uncertainty from all other methods, they are limited to a few fixed ratios of impedances such as 1:1 or 1:10, so they are not suitable for calibration of current shunts that are of arbitrary impedance values (e.g., 6 Ω or 800 mΩ). Furthermore, the bridge topology becomes complicated for quadrature comparison that is required to derive capacitance from calculable resistance standards.

Field of higher impedances is sufficiently covered by the second major topology of bridges, the dual source bridges (DSBs). Good example is the bridge developed at CMI presented in [4]. This bridge offers acceptable accuracy in a full complex plane. However, the accuracy of this topology decreases rapidly when it is used for lower impedances. The problem of the low-impedance accuracy can be solved by using the bridge topology shown in [5] which extends the DSB topology to a four-terminal pair (4TP) by adding several additional sources. However, capabilities of this solution were not yet demonstrated for low impedances at 1 MHz.

Third main topology of bridges suitable mainly for low impedances is called digital sampling bridge, where the ratio of impedances is determined from a voltage drops measured by the digitizers. The general principle of such a bridge is shown in Fig. 1. Extensive review of digital sampling setups

Manuscript received July 9, 2018; revised February 1, 2019; accepted March 26, 2019. Date of publication April 1, 2019; date of current version May 10, 2019. This work was carried out in scope of EMPIR projects TracePQM (15RPT04) and QuADC projects (15SIB04). The projects received funding from the EMPIR Programme co-financed by the Participating States and from the European Union's Horizon 2020 Research and Innovation Programme. The Associate Editor coordinating the review process was Djamel Allal. *(Corresponding author: Stanislav Mašláň.)*

S. Mašláň, M. Šíra, and T. Skalická are with the Czech Metrology Institute, 638 00 Brno, Czech Republic (e-mail: smaslan@cmi.cz).

T. Bergsten is with the Department of Measurement Science and Technology, RISE Research Institutes of Sweden, SE-501 15 Borås, Sweden.

Color versions of one or more of the figures in this paper are available online at http://ieeexplore.ieee.org.

Digital Object Identifier 10.1109/TIM.2019.2908649

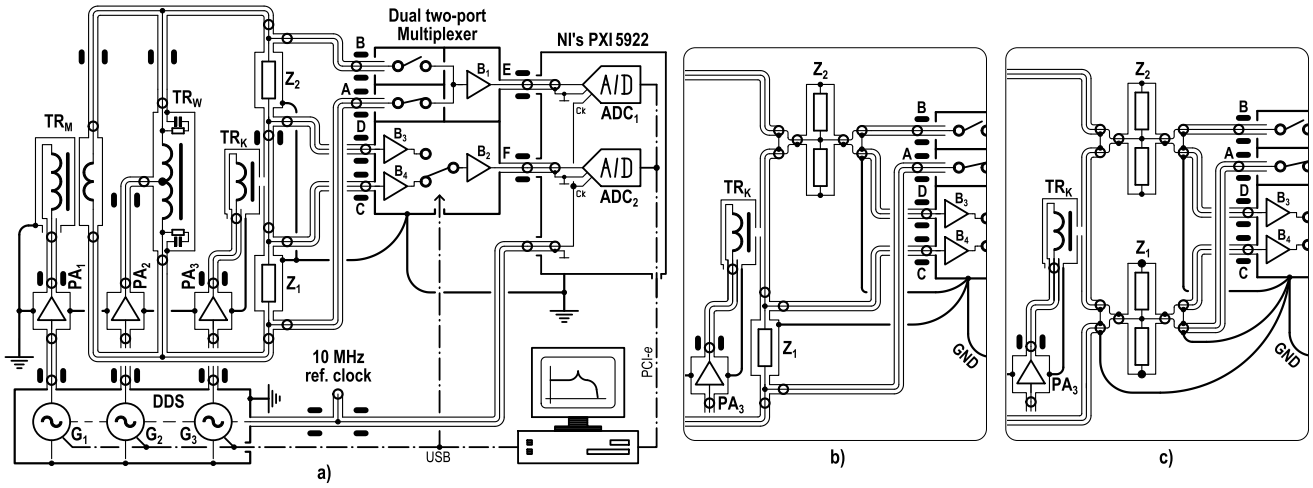

Fig. 2. Full coaxial connection of the 1-MHz impedance bridge. (a) Basic connection for comparing 4TP impedances. (b) Connection for comparing of 4TP to a coaxial shunt. (c) Connection for shunt to shunt comparing. Note the multiplexer internal connection is only principle illustration.

mainly for a frequency band up to few tens of kilohertz can be found in [6].

Several special setups capable of shunt calibration exist for a frequency range above 100 kHz. For example, a phase comparator developed at INRIM [7] based on the isolation transformers should be extendable to 1 MHz. However, usage of this topology was not yet demonstrated for ac–dc difference measurement. Another solution based on the binary inductive current dividers for a phase angle comparison capable to exceed 100 kHz was shown in [8]; however, it was not demonstrated whether it can be used for ac–dc difference as well. Completely different approach for the phase shift measurement was developed at NMIA [9]. It is based on the thermal power comparator and an active guarded isolation transformer. This technique enabled measurement up to 200 kHz.

First wideband bridge-style approach to calibration of the shunts by sampling technique was demonstrated by RISE [10] or [11]. This setup is capable of comparing phase and ac–dc, however, its accuracy decreases when the compared impedances increases due to the nonzero potential at the high-side current shunt. Therefore, it is not optimal for high-accuracy calibration of general impedance standards over few tens of ohms.

In the past years, CMI developed a digital sampling setup for calibration of arbitrary impedance ratios capable to operate up to 100 kHz [12]. The expanded uncertainty below 30 μΩ/Ω was reached. Therefore, this topology was considered as suitable for extension of the frequency range even further up to 1 MHz. Preliminary results of the extension were shown in [13]. This paper focuses on the improvements that had to be done in order to enable operation in the extended frequency range with expanded uncertainty below 100 μΩ/Ω. First, the new multiplexer was designed. Second, the correction scheme was significantly improved to compensate additional errors. Finally, a new fully automatic linearization technique was developed and tested in order to reduce the main source of the bridge errors.

The result is a bridge offering uncertainties comparable to the classic coaxial bridges and DSB topology in an impedance range below 1 kΩ and even better uncertainties below 10 Ω. Furthermore, the presented bridge is fully automatic and capable of calibration of low-impedance standards with arbitrary ratios in a full complex plane, so it can be used for calibration of general impedance standards in R–R, C–C, or R–C topology as well as current shunts. The lower limit of measured impedance is given by a current source, which can deliver up to 3 A, which is sufficient for standards at least down to 50 mΩ. Thus, the bridge is a good low-impedance complement to the precision DSBs for higher impedances.

The bridge was already validated by comparison with ac–dc technique, s-matrix method, and other bridges. Compared to ac–dc method, it is the orders of magnitude faster, compared to s-matrix method for capacitors, it is simpler, and compared to DSB bridges, it does not lose the accuracy when measuring small impedances.

II. 1 MHz Impedance Bridge Hardware Design

The topology of the bridge is extension of the CMI's 100-kHz bridge presented in [12]. The following description of the setup applies for extended frequency range from 10 kHz to 1 MHz. Operation below 10 kHz requires different transformers and chokes as was described in [12].

The principle of operation is shown in Fig. 1. Full coaxial connection and its modifications for non-4TP impedances (shunts) are shown in Fig. 2. The compared impedances Z_1 and Z_2 are supplied via isolation transformer TR_M from a generator G_1 amplified by an amplifier PA_1. The voltage drop between the L_{POT} terminals of the compared impedances Z_1 and Z_2 is eliminated by the voltage injected via the transformer TR_K supplied from a generator G_3 amplified by an amplifier PA_3. From a convention, the circuit will be called Kelvin in the following text. The potentials of the L_{POT} terminals related to the ground are set to 0 V by the last generator G_2 amplified by an amplifier PA_2. This circuit will be called Wagner in the following text. The Wagner voltage is injected via an auxiliary autotransformer TR_W to ensure low source impedance supply to both arms of the bridge. This is needed because slight changes in the multiplexer input

shunting impedances when paths are switched. By lowering the source impedance, the H_{POT} voltage changes due to the varying load changes are minimized. The transformer TR_W is a bifilar winding binary divider on MAGNETEC core M-451 with a total of 18 turns.

A. Bridge Supply

All three generators are realized by a custom designed direct digital synthesizer (DDS). It is based on the 16-bit D/A converters LTC1668 running at fixed 50 MSa/s equipped by a fourth-order Butterworth low-pass filter with cutoff frequency of 4 MHz. The DDS uses dithering, so output voltage regulation has effective vertical resolution of 18-bits. The tuning words are 63-bit wide, so it is very simple to achieve coherent sampling for the setup, as it is possible to generate frequency with very fine step. Spurious-free dynamic range (SFDR) relative to fundamental (carrier) is better than −87 dB up to 1 MHz. The custom DDS also ensure continuous output voltage regulation without attenuator switching that would make balancing more complicated due to the gain and phase jumps. All three power amplifiers are based on the power operational amplifiers LT1210 with additional cascaded feedback from AD8065 amplifiers to improve their transfer stability. Amplifiers can generate rms voltage of 9 V (or 18 V in a full-bridge mode) and rms current 1 A up to several megahertz. SFDR of the amplifiers is below −85 dB at 100 kHz and −70 dB at 1 MHz at full load.

The most challenging component of the bridge supply design were the transformers. Numerous designs were tested for the high-frequency range from 10 kHz to 1 MHz. Currently, the main transformer TR_M shown in Fig. 4 is based on the MAGNETEC NANOPERM tape wound cores M-451 with permeability $\mu_r = 8000$. The cores were rewound to cross section of 15×10 mm and inner diameter of 13 mm. Primary winding is made of ten turns of copper strip 5×0.15 mm split into two sections on the opposing sides of the toroid. Both shields are made from a thin copper foil. Secondary is made of two turns of copper strip 8×0.3 mm, one turn over each primary section as tight as possible to maximize coupling. The Kelvin transformer TR_K is of similar design except primary has total of eight turns and the two secondary turns are connected in parallel. The connection to standards is realized via the 4-mm coaxial cables with silicone dielectric. Two cables are connected in parallel, so the resulting shorted loop impedance is just around 100 nH/m and at the same time the joint stays very flexible. The coaxial leads from the transformers are only 7 cm long to reduce the supply loop impedance. The whole supply loop can deliver 5 A up to 200 kHz and 1.6 A at 1 MHz to total load of 0.5 Ω. With PA_1 and PA_3 in the full bridge mode, the maximum current at 1 MHz exceeds 3 A. SFDR measured at the testing shunts at full current was below −80 dB at 100 kHz and below −63 dB at 1 MHz. Note the transformers have two shields, which is critical at least for operation above 100 kHz. Effectiveness of the shielding was tested by injecting common-mode voltage to the primary winding. The second shield reduced the changes in the measured ratio below 0.5 μV/V at 100 kHz and below 2 μV/V at 1 MHz compared to over 100 μV/V with a single shield.

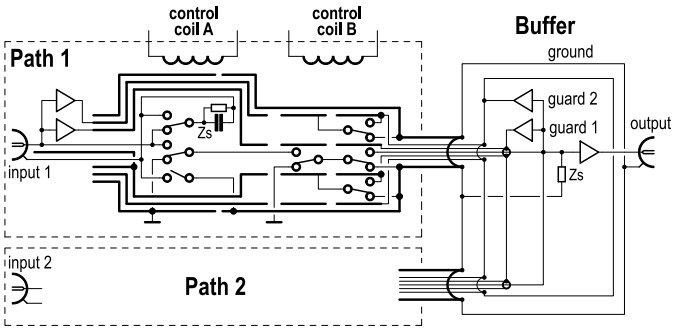

Fig. 3. Internal structure of the multiplexer primary channel. Bold lines in the circuit represent shields from outer to inner one: Ground, Guard 2, and Guard 1.

B. Digitizer

The bridge uses digitizer National Instruments PXI 5922 (16-bit resolution at 15 MSa/s) as it offers high resolution and sufficient bandwidth for the full operating range. The digitizer channels operate in single-ended mode to suppress the common mode rejection problems. Good antialiasing filter implemented in PXI 5922 is important to suppress not so good SFDR of the bridge supply. Tests were made showing even for 3 MHz, −63-dB spur in 1-MHz signal appeared in the spectrum with amplitude below −120 dB. Furthermore, the ratio of sampling to operating frequency is chosen such the alias never overlaps with analyzed harmonic.

C. Multiplexer

The key difference from the 100-kHz bridge [12] is the multiplexer which is used to switch between the high terminal voltages of the compared impedances Z_1 and Z_2. It was decided to use a passive input topology with the reed contacts same as in [12] as it proved to withstand tens of millions of switching cycles without any noticeable effects on its properties. However, it had to be significantly improved to allow operation at 1 MHz. The multiplexer has two channels. Primary channel for the H_{POT} terminals of the standards and secondary channel for the L_{POT} terminals. Each channel has two input paths (one for each compared standard). Both channels can be controlled independently. Properties of the bridge are defined mainly by the primary channel of the multiplexer. Both input paths of the primary channel are fully passive and a buffer is placed at the output of the multiplexer. Thus, both input paths have identical nonlinearity, which is crucial feature that is exploited by the linearity calibration process. It also enables to use the multiplexer for various high-accuracy differential measurements.

The simplified internal structure of the primary channel of the multiplexer is shown in Fig. 3. Each input path consists of three groups of the reed contacts soldered on the 10-cm-long printed circuit board (PCB). The reeds are wrapped around by three shields (two guards and ground). Two independent control windings are wound on top of the shields. The windings are energized sequentially to prevent temporary shorting of the

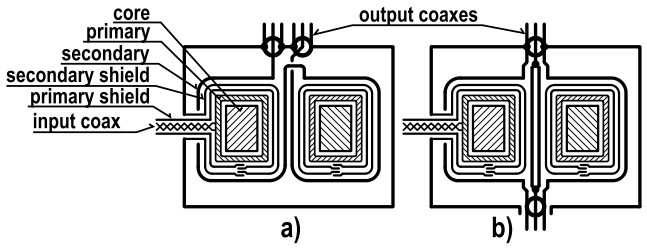

Fig. 4. Construction of supply transformers TR_M and TR_K. (a) Main transformer. (b) Kelvin transformer.

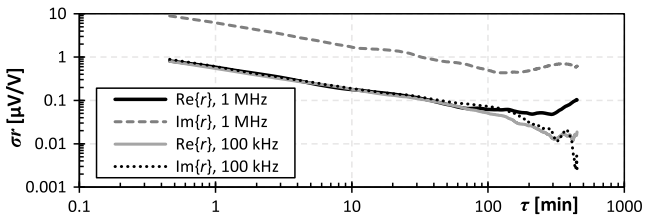

Fig. 5. Stability analysis of the bridge primary channel. Allan deviation of the input differential transfer. Real and imaginary components of the interchannel complex transfer $\hat{r}$ are shown for two operating frequencies.

input during the relay transitions. Constant input admittance independent on the selected multiplexer path is ensured by the substitution RC network Z_S which is connected whenever the path is inactive. Its value is set so that the inactive path has nearly identical input admittance as the active path (difference is below 0.2 pF). Critical task for the 1-MHz operation was reduction in the multiplexer shunting capacitance which was achieved by use of the multiple guards. First, there is a guard of the front stage (left) supplied from the guard buffers based on the AD8065 amplifiers with floating supply permanently connected to the input. Next, there is a rear guard (right) supplied permanently from the output guard buffers also based on the AD8065. Finally, there is a third guard section in the middle of the relay chain which is supplied from the output guard buffers, but only when the path is active. Otherwise, it is grounded in order to reduce the crosstalk from the second path. Guard is two-staged in order to improve its accuracy with respect to the capacitive loading. Outer guard (guard 2) drives total capacitance over 100 pF, so its accuracy is limited, whereas the inner guard (guard 1) drives apparent capacitance only some 15 pF so it follows the live signal more accurately. Note the guard drivers had to be properly compensated for the capacitive loading. Any resonant overshoot on the guard shields is not permissible, otherwise the positive feedback via the large guard-input capacitance may cause oscillations of the output buffer. The eventual oscillations in the bridge circuit were also suppressed by placing the series RC snubber networks between the arms of the transformer TR_W and ground (see Fig. 2). At the selected place, RC snubber networks do not affect the measurement. The values of R and C were based on the properties of the buffer and selected empirically to minimize the chance of oscillations.

The output buffer B_1 of the primary channel is necessary to ensure insensitivity to the frequency-dependent input impedance of the digitizer input. Note eventual voltage dependence of the digitizer input impedance will become part of the digitizer nonlinearity, which is compensated by linearity calibration process. The buffer is of the same topology as presented in [14] and it has input shunting capacitance less than 1 pF. Because of the guards and the buffer, the total capacitance distributed over the whole input path is approximately 8 pF and the dc resistance is 1 MΩ. Most of the capacitance is caused by the grounded leads of the reeds in the relay chain as shown in Fig. 3, so it cannot be prevented. The series loop impedance due to the paralleled reed contacts is approximately 1 Ω. This ensures minimum insertion loss and phase difference and, thus, also good stability of the multiplexer transfer. Stability of the input differential transfer is shown in Fig. 5. Minimum of the Allan deviation occurred for $\tau \approx 3$ h. The total switching time from the one path to the another is below 30 ms, which enables fast time multiplexed measurements.

The secondary channel of the multiplexer for measurement of the L_{POT} voltages is not critical because it is used as a null detector. Therefore, it is designed with ordinary analog video switch DG642 and low-noise operational amplifiers LT1128 at the inputs (B_2 and B_3) and output (B_4).

D. Chokes

Chokes placement is shown in Fig. 2. The placement of the chokes is based on the simulation of the whole coaxial network including multiplexer in SPICE software (SW). Several compromises had to be made to cover at least the desired range 10 kHz–1 MHz since requirements for operation at high-frequency (short cables with low shunting capacitances) contradicts the requirements for operation at low frequency (large inductances). The frequency below 10 kHz requires larger chokes as shown in [12]. Chokes on input cables to the multiplexer are all made of three turns on MAGNETEC M-102 cores and have inductance of more than 500 μH. Choke for the main transformer is made of four rings M-102 (250 μH). The unusual choice to place the choke in series with the Kelvin transformer TR_K (four rings M-102) and the ground lug around it was made because significant voltage drop appears between the shields of the standards at higher measurement currents. This would be normally acceptable if the input chokes to the multiplexer are large enough. In this case, they cannot be extended enough to suppress the unwanted current flow via the multiplexer input cables shields. The SPICE simulation showed the errors introduced this way would easily exceed 50 μV/V at 10 kHz. The errors in the selected choke topology dropped below 1 μV/V up to 100 kHz and below 2 μV/V at 1 MHz.

III. Balancing Procedure and Data Processing

The whole data processing and balancing technique is identical to the one presented in the 100-kHz bridge [12] so it will be described only briefly. The digitizer always operates with coherent sampling, so the vectors of the impedance terminal voltages are obtained using ordinary Fourier transform with rectangular window. The multiplexer has two channels. Primary channel for high-potential (H_{POT}) terminals and secondary for low-potentials (L_{POT}) terminals of the compared standards. The balancing procedure cannot steadily reach

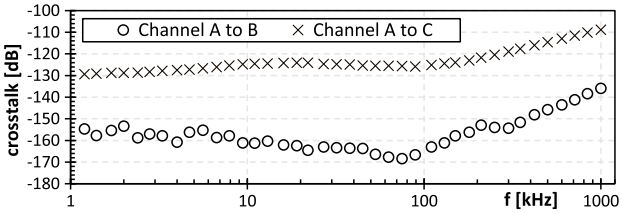

Fig. 6. Measured crosstalk between the inputs A and B of the primary multiplexer channel and between primary and secondary channels (inputs A and C). Measured with 50-Ω source impedances.

needed submicrovolt levels at the L_{POT}, so the L_{POT} voltages are recorded along with the H_{POT}. Thus, four voltage vectors are obtained for each measurement cycle n: 1) high potentials $\hat{U}_{H1}(n)$ and $\hat{U}_{H2}(n)$ and 2) low potentials $\hat{U}_{L1}(n)$ and $\hat{U}_{L2}(n)$. The balancing voltages are intentionally randomized, so the L_{POT} voltages randomly oscillates around zero potential in order of tens of microvolts for each cycle n. After at least three measurement cycles are done, the H_{POT} voltages are assumed to be linear functions of L_{POT} voltages

$$\hat{U}_{H1}(n) = f_1(\hat{U}_{L1}(n)), \hat{U}_{H2}(n) = f_2(\hat{U}_{L2}(n)). \quad (1)$$

The intercepts of the functions $f_1()$ and $f_2()$ obtained by the least square method are equal to voltage drops at the standards Z_1 and Z_2. This simple technique ensures stable reading of the voltage to order of μV/V after few measurement cycles. Another side effect is the bridge does not need to be balanced below few tens of microvolts of residual voltages, which improves the measurement speed.

IV. Corrections

The correction scheme of the bridge had to be significantly improved in order to reach low uncertainty of the measurement at 1 MHz. Following paragraphs will describe applied corrections.

A. Crosstalk Corrections

Total crosstalk between the paths of the primary multiplexer channel is below −136 dB at 1 MHz as shown in Fig. 6. It is measured and corrected to value less than −145 dB in a full range of frequencies. More important is the correction of the crosstalk between the primary and secondary channels, which is mostly caused by the limited channel separation of the 5922 digitizer channels. This crosstalk can easily reach −110 dB. Therefore, the bridge SW applies the primary to secondary channel correction as well to a resulting residual crosstalk below −145 dB. Therefore, the errors introduced by the residual crosstalks are below 1 μV/V even for 16:1 ratio of measured impedances.

B. Differential Transfer Correction

The most important correction is differential transfer error of the inputs (primary channel of the multiplexer). Due to the very low shunting capacitances, the differential real and imaginary transfer error does not exceed 10 μV/V at 1 MHz.

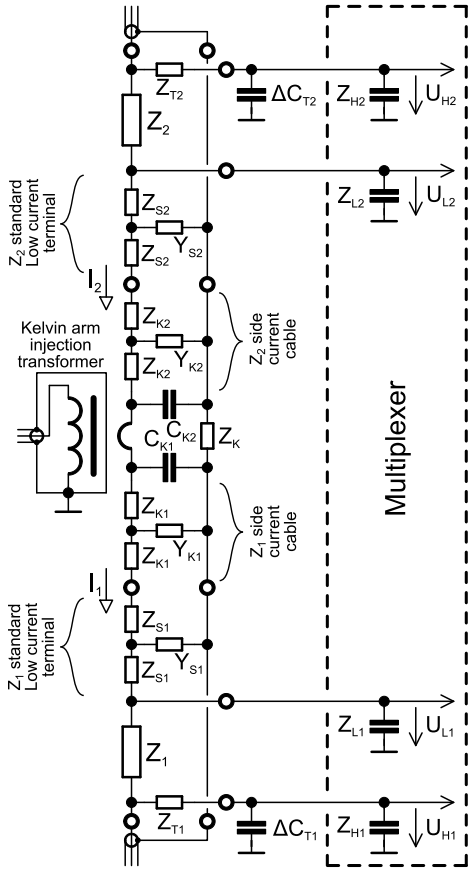

Fig. 7. Model of the Kelvin circuit of the bridge.

However, it is slightly dependent on the drive impedance of the Wagner circuit due to the small changes of multiplexer input impedance when the paths are switched. Therefore, the correction is not measured by simply connecting the primary channel inputs together and measuring the transfer difference. Instead, they are measured in-circuit with two near valued resistors connected as for normal measurement. First, the frequency dependence of Z_1 and Z_2 ratio $\hat{r}_{0a}(f)$ is measured with two near valued resistors Z_1 and Z_2. Then, the impedances Z_1 and Z_2 are swapped and another frequency dependence $\hat{r}_{0b}(f)$ is measured. Both measurements are combined using the following formula:

$$\hat{r}_0(f) = \hat{r}_{0b}(f) \cdot \sqrt{\frac{\hat{r}_{0a}(f)}{\hat{r}_{0b}(f)}} \quad (2)$$

where $\hat{r}_0(f)$ is the desired interchannel transfer error to be used as a correction. This method reduces the interchannel errors below 1 μV/V in full range of frequencies.

C. Kelvin Circuit Correction

Kelvin circuit is one of the problematic parts of impedance bridges operating and higher frequencies. The model of the whole Kelvin circuit is shown in Fig. 7. Whenever the injection circuit, its cables Z_{K1}, Y_{K1} and Z_{K2}, Y_{K2}, or even the internal low-current terminal (L_{CUR}) impedances Z_{S1}, Y_{S1} and Z_{S2}, Y_{S2} are not identical, the currents I_1 and I_2 flowing through

the impedances Z_1 and Z_2 will not be equal. Thus, the whole Kelvin circuit was modeled and user of the bridge must also measure or estimate the impedances of the current terminals of compared impedances. The operating SW of the bridge uses this model and the terminal impedances to calculate the correction by solving the equivalent circuit shown in Fig. 7. This correction can easily reach over 30 μV/V for special adapters from coaxial shunts to 4TP.

D. Loading Effect Correction

Critical correction for the measurements above 100 kHz is the loading effects of the H_{POT} terminals of the compared impedances Z_1 and Z_2 (see Fig. 7). The series inductances Z_{T1} and Z_{T2} of the H_{POT} terminals in combination with the input admittances Z_{H1} and Z_{H2} cause rise in the measured amplitude due to the resonance, whereas the resistive component of Z_{T1} and Z_{T2} lead to small changes in the phase shifts. The phase errors are almost immeasurable; however, the gain errors can easily reach over 100 μV/V at 1 MHz and the effect grows with the square of frequency. Thus, the operating SW of the bridge evaluates the terminal series impedances Z_{T1} and Z_{T2}. The H_{POT} terminals are connected to the bridge via Tee-splitters so an additional loading impedances ΔC_{T1} and ΔC_{T2} can be connected to the H_{POT} terminals. First, the ratio $\hat{r}_0$ of the impedances Z_1 and Z_2 is measured with ΔC_{T1} and ΔC_{T2} disconnected. Then, the measurement is repeated with additional known loading impedance ΔC_{T1} in order to obtain $\hat{r}_1$. Finally, the ΔC_{T2} is connected, ΔC_{T1} disconnected, and ratio $\hat{r}_2$ is obtained. The impedances Z_{T1} and Z_{T2} are calculated by the SW using formulas:

$$\hat{Z}_{T1} \approx \Delta\hat{C}_{T1}\frac{1-\hat{r}_1/k_0}{\hat{r}_1/\hat{r}_0},\ \hat{Z}_{T2} \approx \Delta\hat{C}_{T2}\frac{1-\hat{r}_2/k_0}{\hat{r}_2/\hat{r}_0}. \quad (3)$$

The typical values of $\hat{Z}_{T1}$, $\hat{Z}_{T2}$ and also $\hat{Z}_{S1}$, $\hat{Z}_{S2}$ range from a few nanohenry up to tens of nanohenry for standards with coaxial connections inside or various shunt to 4TP adapters. These values are used together with the known input shunting admittances of the primary channel of the multiplexer (including the cables) to correct for the loading effect using formula

$$\hat{r}' = \frac{\hat{U}_{H2}}{\hat{U}_{H1}} \cdot \frac{\hat{Z}_{H1}}{\hat{Z}_{T1}+\hat{Z}_{H1}} \cdot \frac{\hat{Z}_{T2}+\hat{Z}_{H2}}{\hat{Z}_{H2}} \quad (4)$$

where $\hat{U}_{H1}$ and $\hat{U}_{H2}$ are the measured voltage drops on standards and $\hat{r}'$ is the corrected ratio of impedances.

E. Linearity Correction

The most important correction is the linearity correction, i.e., correction of the nonlinear amplitude transfer of the bridge inputs. Examples of the errors caused by the nonlinearity are shown in Fig. 8. The measurement of the bridge error for the impedance ratio 10:1 showed the error varies more than 100 μV/V at 1 MHz. In the 100-kHz bridge [12], the amplitude transfer was measured by simulating the known impedance ratio by a multitap IVD. However, such process was very time-consuming and required manual operation of the IVD for a whole day. Furthermore, at higher frequencies, the accuracy of the IVD was a limiting factor. Therefore, a more effective and fully automated solution was developed and tested. The method is based on the pair of known impedances (or eventually IVD with single fixed ratio, e.g., 1:10).

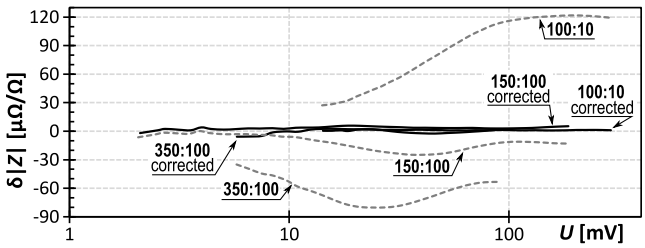

Fig. 8. Measured errors of the bridge ratio at 1 MHz as a function of measurement voltage U for various resistor ratios: 100:10 Ω, 150:100 Ω, and 350:100 Ω. Dashed traces: uncorrected errors. Bold traces: same ratios after linearity correction.

First, the calculable resistors (in our case based on the design [15] with values 100 and 10 Ω) were connected to the bridge. The voltage dependence of their ratio was measured for a given frequency as shown in Fig. 8. This measurement itself can be used to correct only the 10:1 or 1:10 ratios. However, it is possible to obtain the amplitude transfer of the bridge inputs by a simple mathematical processing. The method exploits the fact both paths of the primary channel of the multiplexer have identical nonlinearity. Thus, the measured ratio of the bridge together with the effect of the nonlinear amplitude transfer of the channels can be expressed by the following equations:

$$\hat{U}_1' = \hat{U}_1 \cdot \left\{1 + g(|\hat{U}_1|)\right\} \quad (5)$$

$$\hat{U}_2' = \hat{U}_2 \cdot \left\{1 + g(|\hat{U}_2|)\right\} \quad (6)$$

$$\hat{r} = \frac{\hat{U}_2}{\hat{U}_1} \cdot \left\{1 + g(|\hat{U}_2|) - g(|\hat{U}_1|)\right\} \quad (7)$$

where $\hat{U}_1$ and $\hat{U}_2$ are the actual voltage drops at the impedances Z_1 and Z_2, $\hat{U}_1'$ and $\hat{U}_2'$ are the measured voltages distorted by nonlinear amplitude transfer $g()$ of the bridge. The ratio $\hat{R}$ of the calibrating impedance standards Z_1 and Z_2 is known from the calculable properties of the resistors, so a set of equations can be defined based on the formula

$$\left|\frac{\hat{U}_2(n)}{\hat{U}_1(n)}\right| \cdot \left\{1 + g(|\hat{U}_2(n)|) - g(|\hat{U}_1(n)|)\right\} = |\hat{R}| \quad (8)$$

where n is represented as single point in the measured voltage dependence in Fig. 8, i.e., the following system is created:

$$\left|\begin{array}{l} \left|\dfrac{\hat{U}_2(1)}{\hat{U}_1(1)}\right| \cdot \left\{1 + g(|\hat{U}_2(1)|) - g(|\hat{U}_1(1)|)\right\} \\ \left|\dfrac{\hat{U}_2(2)}{\hat{U}_1(2)}\right| \cdot \left\{1 + g(|\hat{U}_2(2)|) - g(|\hat{U}_1(2)|)\right\} \\ \cdots \\ \left|\dfrac{\hat{U}_2(N)}{\hat{U}_1(N)}\right| \cdot \left\{1 + g(|\hat{U}_2(N)|) - g(|\hat{U}_1(N)|)\right\} \end{array}\right| = |\hat{R}| \quad (9)$$

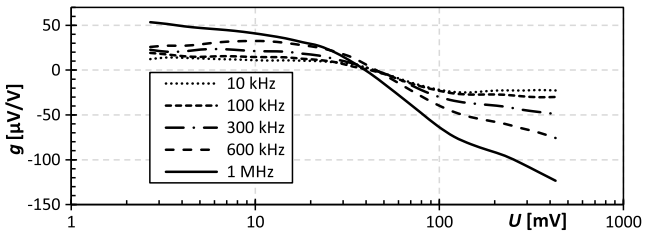

Fig. 9. Calculated nonlinearities (amplitude transfers) for various frequencies.

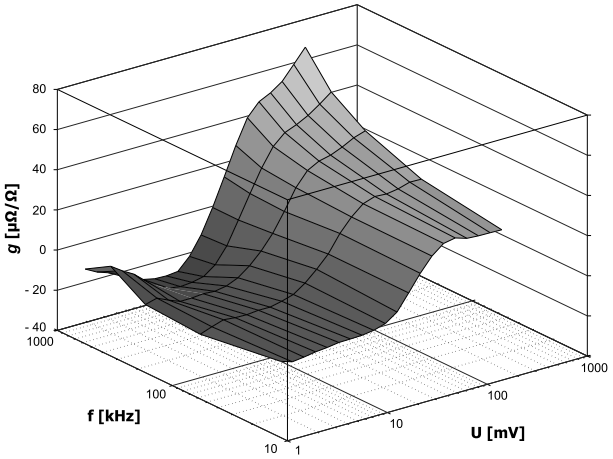

Fig. 10. Calculated nonlinearities (amplitude transfers) shown as 2-D plot.

where N is the total number of points for the calibration of the linearity. It was found empirically N should be at least 40 (optimally over 50) and the voltage points should be logarithmically displaced in the desired voltage range of the bridge. First, the measured voltage dependence was filtered and smoothed to suppress the noise at the low voltages and to eliminate the outliers in the dependence. At the same time, the voltage dependence was upsampled to at least $N = 100$ spots using a spline interpolation. This additional step helped the solver to achieve more repeatable solution. Therefore, for each frequency, there was a system of at least $N = 100$ equations in total and the only unknown in the system is the function $g()$. The solution of the system of (9) [the function $g()$] was found by using a nonlinear least square fitting algorithm. Shape of the function $g()$ was defined as a piecewise function with 30 linear elements logarithmically displaced in the desired amplitude range. Examples of the calculated functions $g()$ for various measurement frequencies are shown in Fig. 9. Complete view in frequency–voltage space is shown in Fig. 10 (note that it is not the same measurement as shown in Fig. 9).

The nonlinearity is unchanged up to approximately 100 kHz. This is consistent with the previous experiences with the 100-kHz bridge [12]. The shape starts to change significantly for the higher frequencies. Therefore, the typical frequency points for calibration of the linearity were chosen to: 20, 100, 300, 600, 800, and 1000 kHz. It was also found the shape of the nonlinearity is affected by the sampling rate of the digitizer PXI 5922, especially at the high-sampling rates. Therefore, the bridge algorithm for selection of the coherent combinations of the operating frequency, sampling rate, and samples count was modified so the bridge uses only a few fixed sampling rates (500 kSa/s for frequencies 10–99 kHz, 1 MSa/s for frequencies 100–299 kHz, and so on). The 5922 is a delta-sigma digitizer and use a series of internal filters to preprocess the results. Different filter coefficients are used for different sampling frequencies. The self-calibration of the 5922 also play its role in the shape of the curve.

Validation of the linearization method and its implementation was performed by numerical simulation and also by measuring the voltage dependencies for various ratios of the resistors and applying the correction according to (7). The example of the achieved suppression of the nonlinear voltage dependence is shown in Fig. 8. All tested ratios reduced their errors roughly below 10 µΩ/Ω in the whole calibrated range.

The same technique was applied to linearize the voltage dependence of the phase angle error. The only difference is the system of equations to solve changes to

$$\text{atan2}(\hat{U}_2(n), \hat{U}_1(n)) + p(|\hat{U}_2(n)|) - p(|\hat{U}_1(n)|) = \text{const.} \quad (10)$$

The right-hand side of the equations is constant because the function $p()$ will only eliminate any relative voltage dependence of the phase angle error, whereas the absolute phase angle error is corrected by the differential transfer correction (see Section IV-B). Therefore, in this case, it is not necessary to know the absolute phase difference of the calibration standards. The only condition is the phase angle of the standards must be independent of the voltage (up to some level of uncertainty). However, practical experiments showed the variation in the phase angle error is negligible compared to other sources of phase uncertainty. Even at 1 MHz, the variation was below 20 ps in the whole voltage range.

The estimated uncertainty of the linearity correction is based on the three main sources. Dominant component is the uncertainty of the calculable resistors pair. Second component is the corrections applied (mainly the loading correction and Kelvin circuit correction). The third component appears at lower voltages due to the noise in the measurement. Note in-depth uncertainty analysis is planned for a separate paper together with other sources. However, an empirical estimate was made based on the: 1) repeatability and 2) observed ratios errors for the measurement of arbitrary ratios other than the ones used for the linearization (e.g., 1:3 and 1:5). The total estimated standard uncertainty contribution was estimated to 20 µΩ/Ω at 1 MHz for voltages above 10 mV.

The whole process of linearization is fully automatic and is usually run overnight (roughly 8 h), and the next day, the measured data are automatically processed by a MATLAB script and can be immediately used for new measurements.

Stability of the correction was analyzed and it was found the shape of the nonlinearity changes by more than 10 µΩ/Ω every time the self-calibration of the PXI 5922 is performed due to the self-linearization process of the 5922. Therefore, the PXI 5922 is typically self-calibrated once before linearization and then used for up to 1 week without turning the power off. The observed stability of the corrections is below 10 µΩ/Ω for at least 7 days.

TABLE I

EXAMPLE OF UNCERTAINTY BUDGETS FOR THE MEASUREMENT OF 16:1 RATIO WHEN THE LOWER OF IMPEDANCES HAS VOLTAGE DROP AT LEAST 20 mV. REPEATABILITY ALSO CONTAINS TYPE A UNCERTAINTY FROM THE PROCESSING. * SEE TEXT

Component	Magnitude [μΩ/Ω]		Phase [μrad]	
	100 kHz	1 MHz	100 kHz	1 MHz
Linearity	4	19	16	160
Kelvin circuit	1.5	8	5	50
Input Z variation *	1	9	2	20
Loading effect	0.1	12	6	60
Crosstalk	0.5	0.5	8	8
Coaxial network *	0.7	2.5	0.7	2.5
Repeatability	2	5	3	30
Total	4.9	26	20	180
Total (k = 2)	9.8	52	40	360

V. UNCERTAINTY

In-depth uncertainty analysis based on the modeling of the whole coaxial circuit is planned to a follow-up paper. However, dominant sources were already identified. Examples of the uncertainty budgets for ratios up to 16:1 are given in Table I. The dominant component of the uncertainty is the linearity correction. Next largest component at 1 MHz is the loading effect which may be eventually reduced by using shorter cables. Note the slight variation in the input shunting impedance due to the imperfect balancing of the substituting network Z_S at the input of the multiplexer causes disbalancing of the bridge when changing the paths. It is possible to set the variation below 0.2 pF; however, the capacitance is frequency dependent, so it can be balanced at only one frequency. Therefore, a compromise was made and it is balanced at 800 kHz which leads to nonzero effect at 1 MHz (component input Z variation).

The expanded uncertainty of the impedance for the low-impedance ratios below 1:1.1 is just around 35 μΩ/Ω as the linearity component becomes almost irrelevant.

Component coaxial network is the first estimate of combined errors introduced by the unbalanced currents in the coaxial network obtained from a model of the coaxial circuit and by the imperfect shielding of the transformers. This component will be analyzed deeper in the follow-up paper.

VI. VALIDATION

A first set of validation measurements was performed. A set of measurements of known impedance standards and a small international comparison was carried out to validate the bridge capabilities and assigned uncertainty for the mid range of impedances from 120 mΩ up to 1 kΩ.

A. Basic Tests

First, a series of tests was made at various frequencies to validate the linearization method (see Fig. 8). Another consistency test was performed with three impedance standards: 1 kΩ, 350 Ω, and 3.2 nF. Three complex impedance ratios $\hat{a}$, $\hat{b}$, and $\hat{c}$ were measured between each pair of the impedances. Product $\hat{a} \cdot \hat{b} \cdot \hat{c}$ of the three ratios should be exactly one. The error of the product shown in Fig. 11 showed total deviation below 12 μΩ/Ω and below 50 μrad up to 1 MHz. Note the use of an inductor for this test was not possible due to limited stability of such component, so a resistor was used instead. Similar consistency test was repeated with three shunts with current of 1 A with deviations 30 μΩ/Ω and 50 μrad (see Fig. 12).

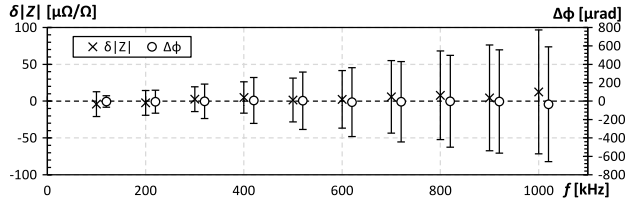

Fig. 11. Magnitude and phase errors of the consistency test with three impedances (see text for details): 1 kΩ, 350 Ω, and 3.2 nF. Voltage at the capacitor was held at 15 mV to prevent its voltage dependence. Uncertainty is expanded to $k = 2$.

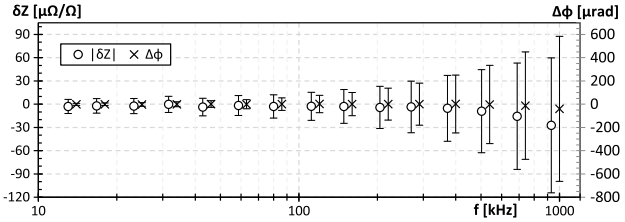

Fig. 12. Magnitude and phase errors of the consistency test with three shunts measured with current 1 A (see text for details). Used shunts: 600 mΩ (1 A), 200 mΩ (3 A), and 120 mΩ (5 A). Uncertainty is expanded to $k = 2$.

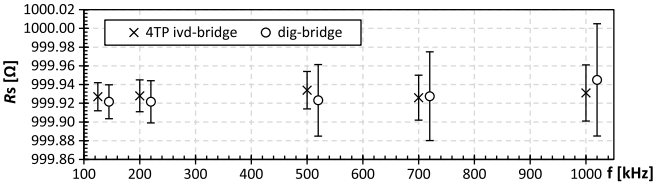

Fig. 13. Measurement of 1-kΩ resistor by the new sampling bridge (dig-bridge) in 1:10 ratio and by CMI's digitally assisted bridge [3] (4TP ivd-bridge) in 1:1 ratio. Uncertainty is expanded to $k = 2$.

One of the key measurements in impedance metrology is the quadrature *RC* comparison. Thus, an Agilent 16384A air capacitor 1 nF was compared to the various resistance and capacitance standards and it was also measured by the s-matrix technique which served as a reference value. Results of the capacitance and loss factor measurements are shown in Fig. 14. The deviations from the reference value at 1 MHz were below 30 μF/F which is within the expanded uncertainty 50–60 μF/F. Note the dominant source of loss factor uncertainty was the uncertainty of the time constant of the reference calculable resistors [15].

Test of 1:10 ratio R–R measurement was made with impedance of 1 kΩ which was also calibrated by the 4TP digitally assisted bridge [3]. The deviations between the bridges were below 20 μΩ/Ω as shown in Fig. 13.

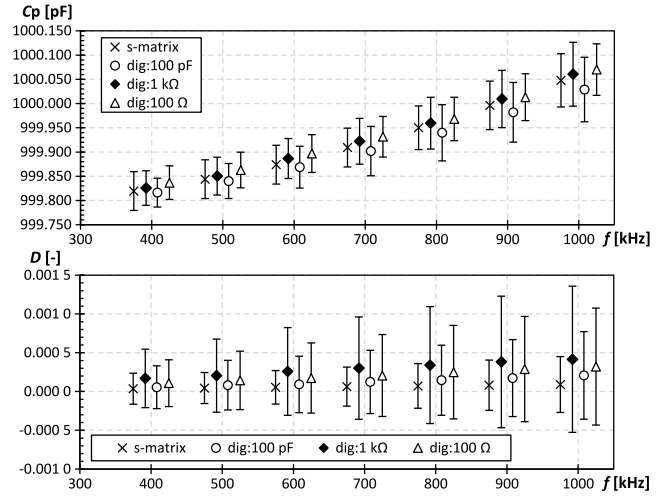

Fig. 14. Comparison of measurement of 1-nF air capacitor Agilent 16384A by several methods. s-matrix: reference value obtained by the s-matrix method. Dig:100 pF: comparison to 100-pF capacitor Agilent 16383A calibrated by s-matrix technique by digital bridge (ratio 10:1); Dig:1 kω: comparison to 1-kΩ standard resistor. Dig:100 ω: comparison to 100-Ω calculable resistor. Measurement voltage was kept at 200 mV at the higher of the two impedances. Uncertainty is expanded to $k = 2$.

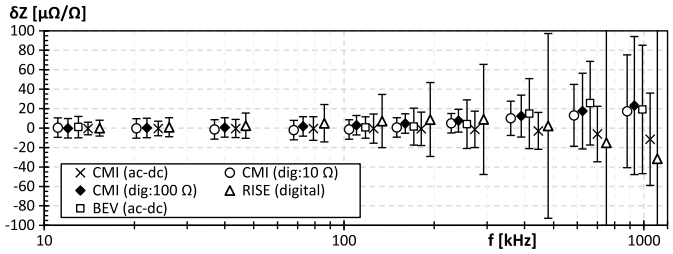

Fig. 15. Comparison of measurement of relative frequency dependence of module of impedance of a 100 mA, 6-Ω current shunt. CMI ac–dc: ac–dc transfer and dc R measurement by CMI at 30 mA. CMI dig:10 Ω: comparison to the 10 Ω calculable resistor by digital bridge by CMI at 30 mA. CMI dig:100 Ω: comparison to the 100-Ω calculable resistor by digital bridge by CMI at 3 mA. BEV ac–dc: ac–dc difference dc R measurement by BEV at 30 mA. RISE digital: comparison to calculable shunts by digital setup. Note the RISE measurement uncertainty reaches 200 $\mu\Omega/\Omega$ at 1 MHz. Uncertainty is expanded to $k = 2$.

B. Comparison

In order to validate the bridge capability to measure low impedances, a small interlaboratory comparison was organized in scope of EMPIR project TracePQM [16]. Several current shunts were measured by the traditional ac–dc technique and by the digital sampling setups in terms of ac–dc difference and phase angle. The comparison for higher current shunts is still running and the details will be presented at a standalone paper. However, the results of the first measurement of 100-mA shunt are already available.

The first measurement shown in Fig. 15 was performed with 100-mA coaxial current shunt (CMI construction [17]) with nominal resistance 6 Ω. CMI measured the shunt by means of ac–dc technique and using the digital impedance bridge. The shunt was connected via the coaxial to 4TP adapters for the bridge measurement and compared to the calculable

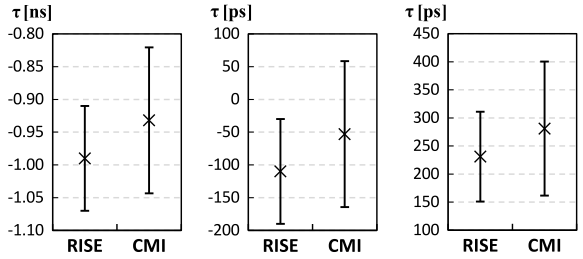

Fig. 16. Comparison of time constants of several coaxial shunts between RISE and CMI. 6-Ω shunt, 2-Ω shunt, and 0.6-Ω shunt (from left to right). CMI compared the shunts using the digital bridge to the 100 Ω and 10 Ω standards. RISE used digital sampling setup. All measurements were performed at 1 MHz. Uncertainty is expanded to $k = 2$.

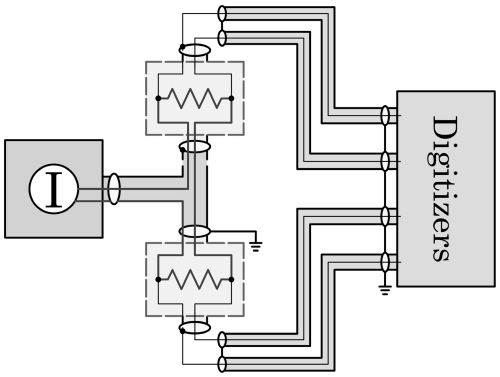

Fig. 17. Digital impedance ratio bridge at RISE. ac current source supplies the current for the two current shunts connected in series using a current T-connector (left). Four digitizer channels sample the voltage signals at high and low potential of both shunts simultaneously.

resistors [15]. BEV measured the shunt by means of the traditional ac–dc difference method.

The current shunt measuring system at RISE [10] consists of an ac current source, a current T-connector, and two two-channel digitizers with sampling frequency up to 15 MHz (Fig. 17). The two current shunts to be compared are connected in series using the current T-connector. As output low of the current source is connected to ground, one shunt will be on high potential. Hence, the two-channel digitizers are used to measure the high and low output voltage potentials of both shunts relative ground. This setup was used for both relative impedance measurements against reference shunts, and for realization of absolute phase and ac resistance [11]. Three independent realizations were carried out and averaged for improved uncertainty.

The deviations of all methods and participants were well within the uncertainty. Note the higher uncertainty of the RISE method is caused by the realization method for ac resistance.

The time constant of the same 6-Ω shunt was compared to the RISE measurement as well (see Fig. 16). The comparison of time constant was repeated for two more shunts of different values. The deviations for all shunts were constant around 55 ps (350 μrad/MHz) which is well within the assigned uncertainties. No significant changes in the differences between CMI and RISE were observed at least from 10 kHz to 1 MHz where the values were measured.

VII. Conclusion

The new digital sampling bridge for frequency band up to 1 MHz optimized for low impedances was developed. Bridge offers uncertainties comparable to the classic coaxial bridges and DSB topology in an impedance range below 1 kΩ and even better uncertainties below 10 Ω. The bridge is fully automatic and capable of calibration of low-impedance standards with arbitrary ratios in a full complex plane, so it can be used for calibration of general impedance standards in R–R, C–C, or R–C topology as well as current shunts. The bridge is a good low-impedance complement to the precision DSBs for higher impedances.

To keep uncertainties low, automatic method of linearity calibration was developed and validated by a set of measurements of impedance standards of known values. The bridge expanded uncertainty at 1 MHz is around 50 μΩ/Ω for the impedance ratios up to 16:1 and voltage drops at least 10 mV. Phase angle uncertainty of the bridge at 1 MHz is below 400 μrad. Measurements of ratios below 1:1.1 showed deviations below 15 μΩ/Ω. Uncertainties of the impedance ratio and phase angle were confirmed by a series of measurements of known impedances and also by an international comparison of current shunts with RISE and BEV.

Future work will be focused on in-depth analysis of the uncertainty, mainly on the contribution of the imperfect current balance in the coaxial network. The uncertainty needs to be analyzed using a full circuit model of the bridge coaxial network combined with the digital processing algorithms of the bridge itself.

Future development of the bridge hardware (HW) will be focused on the improvement of the multiplexer and buffer in order to reach even lower shunting admittances. Also, the integration of additional circuitry to allow automatic compensation of the loading effect is planned. So far performed tests and models suggest the topology is capable to operate at least up to 2 MHz. Operation at 10 MHz with this topology does not seem to be practical because the loading effects would increase the uncertainty to at least 0.1 %.

Acknowledgment

The authors would like to thank V. N. Zachovalová from CMI and M. Garczocz from BEV for their participation in the international comparison of the current shunts. The validation of the bridge capabilities at low impedances and high frequencies would not be possible without their effort.

References

[1] S. A. Awan, B. P. Kibble, I. A. Robinson, and S. P. Giblin, "A new four terminal-pair bridge for traceable impedance measurements at frequencies up to 1 MHz," *IEEE Trans. Instrum. Meas.*, vol. 50, no. 2, pp. 282–285, Apr. 2001.

[2] S. A. Awan and B. P. Kibble, "Towards accurate measurement of the frequency dependence of capacitance and resistance standards up to 10 MHz," *IEEE Trans. Instrum. Meas.*, vol. 54, no. 2, pp. 516–520, Apr. 2005.

[3] J. Kučera, R. Sedláček, and J. Boháček, "An HF coaxial bridge for measuring impedance ratios up to 1 MHz," *Meas. Sci. Technol.*, vol. 23, no. 8, 2012, Art. no. 085004.

[4] D. B. Kim, H. K. Lee, and W.-S. Kim, "An impedance bridge measuring the capacitance ratio in the high frequency range up to 1 MHz," *Meas. Sci. Technol.*, vol. 28, no. 2, 2017, Art. no. 025014.

[5] J. Kučera and J. Kováč, "A reconfigurable four terminal-pair digitally assisted and fully digital impedance ratio bridge," *IEEE Trans. Instrum. Meas.*, vol. 67, no. 5, pp. 1199–1206, May 2018.

[6] R. Rybski, J. Kaczmarek, and M. Kozioł, "A PXI-based calibration system for low-value AC resistors," *IEEE Trans. Instrum. Meas.*, vol. 67, no. 4, pp. 905–911, Apr. 2018.

[7] U. Pogliano, B. Trinchera, and D. Serazio. (2011). "Wideband digital phase comparator for high current shunts." [Online]. Available: https://arxiv.org/abs/1110.0866v1

[8] J. Zhang, X. Pan, W. Liu, Y. Gu, B. Wang, and D. Zhang, "Determination of equivalent inductance of current shunts at frequency up to 200 kHz," *IEEE Trans. Instrum. Meas.*, vol. 62, no. 6, pp. 1664–1668, Jun. 2013.

[9] I. Budovsky, "Measurement of phase angle errors of precision current shunts in the frequency range from 40 Hz to 200 kHz," *IEEE Trans. Instrum. Meas.*, vol. 56, no. 2, pp. 284–288, Apr. 2007.

[10] K. E. Rydler, T. Bergsten, and V. Tarasso, "Determination of phase angle errors of current shunts for wideband power measurement," in *Proc. Conf. Precis. Electromagn. Meas.*, Jul. 2012, pp. 284–285.

[11] T. Bergsten and K.-E. Rydler, "Realization of absolute phase and AC resistance of current shunts by ratio measurements," *IEEE Trans. Instrum. Meas.*, to be published.

[12] S. Mašláň, M. Šíra, V. Z. Nováková, and J. Streit, "Digital sampling setup for measurement of complex voltage ratio," *IEEE Trans. Instrum. Meas.*, vol. 66, no. 6, pp. 1355–1363, Jun. 2017.

[13] S. Mašláň, M. Šíra, and T. Skalická, "Four terminal pair digital sampling impedance bridge," in *Proc. Conf. Precis. Electromagn. Meas. (CPEM)*, Jul. 2016, pp. 1–2.

[14] S. Mašláň, M. Šíra, and T. Skalická, "Precision buffer with low input capacitance," in *Proc. Conf. Precis. Electromagn. Meas. (CPEM)*, 2018, pp. 1–4.

[15] S. Mašláň, M. Šíra, and T. Skalická, "Progress on simple resistance standard with calculable time constant," in *Proc. Conf. Precis. Electromagn. Meas. (CPEM)*, 2018, pp. 1–8.

[16] *EMPIR Project Traceability Routes for Electrical Power Quality Measurement*. Accessed: Jan. 29, 2019. [Online]. Available: http://tracepqm.cmi.cz/

[17] V. N. Zachoválová, "On the current shunts modeling," *IEEE Trans. Instrum. Meas.*, vol. 63, no. 6, pp. 1620–1627, Jun. 2014.

Stanislav Mašláň received the master's degree in automation and measurement techniques from the Technical University of Brno, Brno, Czech Republic.

Since 2011, he has been with the Czech Metrology Institute, Brno. He is currently involved in low-frequency impedance measurement and sampling techniques development. He is also involved in the development of the data processing and analysis algorithms, uncertainty analysis algorithms, and in the development of hardware and software for various measurements automation.

Martin Šíra received the M.S. degree in physics and the Ph.D. degree in plasma physics from Masaryk University, Brno, Czech Republic, in 2003 and 2009, respectively. His Ph.D. dissertation was focused on the deposition of thin films and the activation of polymer surfaces in plasmas.

Since 2008, he has been a Metrologist and the Maintainer of quantum voltage standard-Josephson voltage system with the Czech Metrology Institute, Brno. He is involved in developing and improving national standard of voltage.

Tereza Skalická received the M.S. degree in physics from Masaryk University, Brno, Czech Republic, in 2007.

Since 2016, she has been a Metrologist and the Maintainer of quantum voltage standard-Josephson voltage system with Czech Metrology Institute, Brno.

Tobias Bergsten was born in Lund, Sweden, in 1970. He received the M.Sc. degree in engineering physics and the Ph.D. degree in physics, with a focus on Coulomb blockade thermometry, from the Chalmers University of Technology, Gothenburg, Sweden, in 1996 and 2001, respectively.

In 2004, he joined the Spintronics Group, NTT Basic Research Laboratories, Atsugi, Japan, where he was involved in Rashba spin–orbit interference devices. In 2006, he was with the Semiconductor Physics Group, University of Cambridge, Cambridge, U.K., where he was involved in AFM measurements on graphene. In 2009, he joined the Electrical Metrology Laboratory, RISE Research Institutes of Sweden, Borås, Sweden, where he is developing electrical measurement methods.